Assessing the Temporal Transferability of Random Forest Models for Land Use and Land Cover Change Detection

Beste Tavus[1*], Melih Altay[2], Fatih Fehmi Simsek[3], Omer Gokberk Narin[4], Saygin Abdikan[1]

[1] Hacettepe University, Department of Geomatics Engineering, Ankara, Türkiye - (beste.tavus, sayginabdikan@hacettepe.edu.tr)
[2] Hacettepe University, Graduate School of Science and Engineering, Ankara, Türkiye - melihaltay17@hacettepe.edu.tr
[3] TÜBİTAK Space Technologies Research Institute, Ankara, Türkiye - fehmi.simsek@tubitak.gov.tr
[4] Afyonkocatepe University, Department of Geomatics Engineering, Afyonkarahisar, Türkiye - gokberknarin@aku.edu.tr

Keywords: Sentinel-1, Sentinel-2, Machine Learning, Deforestation, Google Earth Engine (GEE).

Abstract

Monitoring land-use and land-cover (LULC) dynamics in rapidly urbanizing regions is critical for sustainable environmental planning. Dynamic metropolitan areas with rapid urbanization, such as Istanbul, Türkiye, are experiencing significant land-cover changes, among which deforestation is one of the most critical. This study presents a Google Earth Engine (GEE)-based framework to monitor LULC changes in Istanbul from 2016 to 2025 by fusing Sentinel-2 optical imagery, Sentinel-1 SAR and topographic data. From these datasets, a feature set—including spectral bands, vegetation indices, SAR backscatter metrics, and topographic variables—was derived and used to train a Random Forest (RF) baseline model on 2016 Land Parcel Identification System (LPIS) reference data. The baseline model was then applied across the time series to assess its temporal transferability, overcoming the limitation of up-to-date ground-truth data. The baseline model achieved an overall accuracy of 72%, calculated using a validation dataset derived from the LPIS reference data. Feature importance analysis revealed that structural variables—particularly DEM and SAR metrics—were the primary contributors to the classification, used in combination with optical features. Time-series results indicate a cumulative decline of 231 km² in agriculture and 379 km² in forest cover during the study period, inversely corresponding to urban growth. The results of the study highlight that, although applying a single-year model without independent annual validation data causes certain uncertainties—arising from methods, sensors, or topography (e.g., misclassifications)—the proposed framework is highly practical for monitoring deforestation and urbanization trends in complex landscapes.

1. Introduction

Monitoring land-use and land-cover (LULC) dynamics in complex landscapes is essential for effective land management and biodiversity conservation and climate change mitigation. Rapid urbanization, population growth, and climate-related factors increasingly affect forest and agricultural ecosystems, making timely and accurate information on land-cover change critical for sustainable regional planning (Zhu et al., 2020). Metropolitan areas such as Istanbul, Türkiye represent highly heterogeneous landscapes, where urban expansion, deforestation and agricultural decline occur simultaneously.

Remote sensing, particularly optical and radar satellite imagery, has become an important tool for mapping and monitoring forest dynamics over large areas. Optical satellite imagery, particularly Sentinel-2, offers high spectral and spatial resolution, enabling discrimination of vegetation, agricultural areas, and built-up surfaces (Ozdemir et al., 2024; Ye et al., 2021; Zhang et al., 2022).

However, limitations such as cloud contamination, seasonal phenological variability, and spectral overlaps between different classes can reduce classification accuracy and temporal consistency in long-term analyses (Bullock et al., 2020). Synthetic Aperture Radar (SAR) data from Sentinel-1 provide complementary structural information and enable cloud-independent observations that enhance the detection of forest and urban features (Lehmann et al., 2015; Reiche et al., 2018; Watanabe et al., 2021).

Previous research has shown that fusing SAR and optical satellite imagery enhances land cover classification performance by leveraging complementary information from different sensor types. Optical data provide rich spectral signatures that facilitate discrimination among vegetation, water, bare soil, and built-up areas, while SAR data contribute structural and textural information that is largely independent of atmospheric conditions such as cloud cover (Mao et al., 2025; Watanabe et al., 2021). For example, a recent study using the SEN12MS dataset demonstrated that early fusion of Sentinel-1 SAR and Sentinel-2 optical data achieved overall accuracies above ~88 % in scene-level LULC classification, outperforming alternative fusion strategies and single-sensor models across diverse land cover types (Irfan et al., 2025).

Another study shows the complementary use of Sentinel-1 and Sentinel-2 data has been shown to substantially improve classification results: Support Vector Machine (SVM) achieved an overall accuracy (OA) of 0.91 and Random Forest (RF) achieved an OA of 0.81 when using the fused dataset, compared to accuracies (~0.69) with individual Sentinel-2 or Sentinel-1 inputs alone. Similar benefits have been reported in agriculture, where the integration of Sentinel-1 backscatter with Sentinel-2 spectral bands and topographic data increased OA to 89.1 %, representing a significant improvement relative to classifications based on single sensors (Van Tricht et al., 2018).

Istanbul, the study area of this research, represents one of the most dynamic metropolitan regions, characterized by complex forests, agricultural lands, urban areas, and water bodies. Rapid

* Corresponding author

infrastructure development, population growth, and economic expansion are accelerating land-use changes, creating major obstacles for ecological sustainability and urban planning. Understanding these spatial and temporal dynamics of LULC change in this context is therefore essential for informed decision-making, regional planning and sustainable land management.

In this study, multi-source Sentinel-1 SAR, Sentinel-2 optical data and topographic data were leveraged within the Google Earth Engine (GEE) platform to monitor LULC changes in Istanbul over the 2016–2025 period. An RF baseline model was trained using a single reference year to generate annual land-cover maps, with particular attention given to forested, agricultural and urban areas due to their ecological and socio-economic importance.

2. Materials and Methods

2.1 Study Area

The study area, Istanbul, ranges from 0 to 500 meters above sea level and has a diverse topography, ranging from coastal areas to low hills. As shown in Figure 1, the majority of the area is covered by forests and agricultural lands, while urban areas cover about 23%, mainly in the southern parts according to the Land Parcel Identification System (LPIS). Water bodies and roads cover smaller portions of the landscape, and urban areas are mostly located around forest and agricultural zones (Simsek and Durduran, 2017).

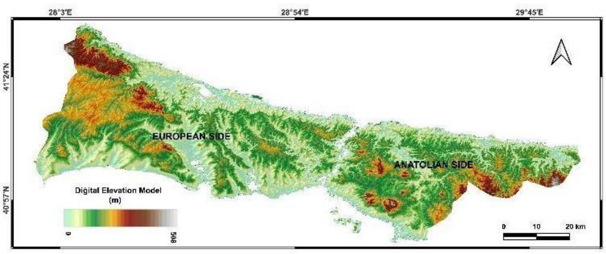

Figure 1. Digital elevation model of Istanbul.

2.2 Methodology

The overall methodological workflow of the study, which was entirely conducted in Google Earth Engine (GEE) platform, is given in Figure 2 (Gorelick et al., 2017).

To complement the optical data, Sentinel-1 GRD images acquired between July and September 2016 were radiometrically terrain-corrected (RTC) to minimize topography-induced backscatter distortions, and a summer median composite was generated to ensure seasonal consistency with the Sentinel-2 dataset. Backscatter outliers were masked, and a Lee speckle filter was applied to the median composite to reduce speckle noise. Sentinel-1 GRD images were filtered using a Lee speckle filter to reduce radar noise while preserving edges and textural information. Only data from the descending orbit with an Interferometric Wide (IW) instrument mode were utilized to ensure consistent geometry.

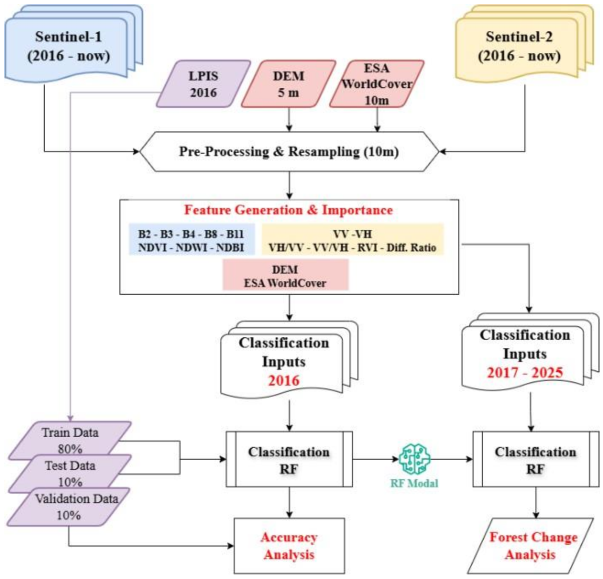

Figure 2. The overall methodological workflow.

Several SAR-derived indices, including VV/VH, VV − VH, difference ratio and the Radar Vegetation Index (RVI), were subsequently generated using sigma-naught backscatter values (Eisfelder et al., 2024). The final feature stack was created by integrating Sentinel-1&2 spectral bands and indices, together with ancillary datasets including a 5 m DEM and the ESA WorldCover LULC map, resulting in a multi-source dataset at 10 m spatial resolution. While the ESA WorldCover dataset was used as an auxiliary input feature to improve the feature space and class separability, LPIS data were used as the only ground-truth dataset for training, testing, and validation. The overall dataset utilized in this study is summarized in Table 1 along with its corresponding usage.

	Bands	Features	Usage
Sentinel-1	VV &VH	VV/VH, VH/VV, RVI, VV−VH	Feature Generation
Sentinel-2	B2, B3, B4, B5, B8, B8A, B11, B12	NDVI, EVI, NDWI, RNDWI, NDBI, RWI, SWI	
DEM	Elevation (m)	-	
ESA WorldCover	Land Cover map	Land-cover class	
LPIS	-	-	Train, Test & Validation

Table 1. The overall dataset

To evaluate the relative contribution of each input variable to the classification process, feature importance was extracted from the trained Random Forest model using the built-in variable importance measure based on the mean decrease in impurity (Gini importance) (Menze et al., 2009). The importance scores were normalized by dividing each variable’s contribution by the total importance, resulting in relative importance values ranging between 0 and 1. The analysis included 23 features, comprising Sentinel-2 spectral bands (B2, B3, B4, B5, B8, B8A, B11, B12) and indices (NDVI, EVI, NDWI, RNDWI, NDBI, RWI, SWI), Sentinel-1 bands (VV, VH) and indices (VV/VH, VH/VV, RVI, VV−VH), as well as topographic data (DEM) and ESA World Cover.

The results indicated that topographic information (DEM) provided the highest relative contribution (0.070), followed by SAR backscatter metrics (VH: 0.064; VV: 0.062) and vegetation-related indices such as EVI (0.063) and RVI (0.061). Notably, EVI and RVI exhibited higher importance than the conventional NDVI, highlighting their effectiveness in discriminating dense vegetation and forest structures. Other spectral indices (NDWI, NDBI, and RWI) together with SWIR and Red-Edge bands provided consistent contributions to the classification of water bodies and urban surfaces, supporting the overall robustness of the model across heterogeneous landscapes.

As described by Simsek and Durduran (2017), LPIS data were generated based on agricultural parcel boundaries and high-resolution 2016 orthophoto imagery. The original dataset comprises parcel-level thematic classes including arable land, bare land, urban areas, forest, artificial surfaces, greenhouses, shrubland, tree crops, water bodies, and other officially declared land-use categories. In this study, the original LPIS classes were merged into six main land-cover classes including Agriculture, Bare land, Forest, Urban, Roads, and Water. A stratified random sampling strategy was applied to the LPIS-derived point dataset. Reference points were randomly selected from each of the six land-cover classes to ensure balanced representation across classes. The selected samples were further randomly split into training (80%), testing (10%), and validation (10%) subsets using a systematic randomization procedure, ensuring an unbiased distribution of samples for both model training and objective accuracy assessment (Figure 3). Figure 4 shows the distribution of labeled datasets for training, testing, and validation processes within a specific area.

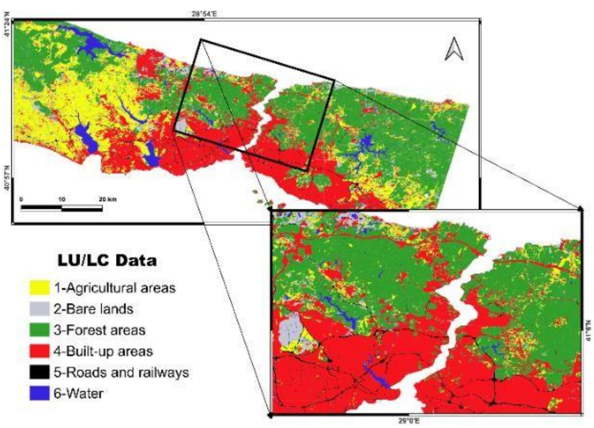

Figure 3. The LULC map from LPIS - 2016 (Simsek and Durduran, 2017).

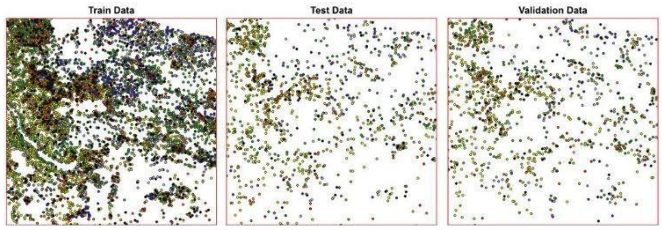

Figure 4. The Labeled dataset for train (80%), test (10%) and validation (10%) zones (Simsek and Durduran, 2017).

The RF classifier was implemented using 200 trees, with four variables per split, a minimum leaf population of two, and a bag fraction of 0.6 to reduce overfitting (Breiman, 2001). Post-classification filtering was applied to enhance the thematic reliability and visual clarity of the classification results. A majority filter was first implemented to reassign isolated pixels according to the dominant class within a defined neighborhood. This was followed by morphological opening and closing operations (focal minimum and maximum), which helped remove small, isolated pixel clusters and smooth class boundaries.

Classification accuracy was evaluated using independent validation samples through confusion matrices, reporting overall accuracy as well as class-specific producer's (PA) and user's (UA) accuracies. Some features and the 2016 land-cover classification map are presented in Figures 5 and 6, while the corresponding accuracy metrics are summarized in Table 2 Using the workflow illustrated in Figure 2, the 2016-trained model was subsequently applied to the 2017–2025 summer datasets without retraining in order to evaluate temporal transferability.

3. Results and Discussion

Some of the features derived from Sentinel-1&2 and ancillary data are presented in Figure 5. The feature importance analysis revealed a clear dominance of topographic and SAR backscatter variables, followed by optical spectral bands and vegetation-related indices. In particular, elevation and radar-derived metrics showed consistently higher contributions compared to several spectral indices. Features with very low importance (<0.05) were excluded from further modeling in order to reduce redundancy and improve model efficiency.

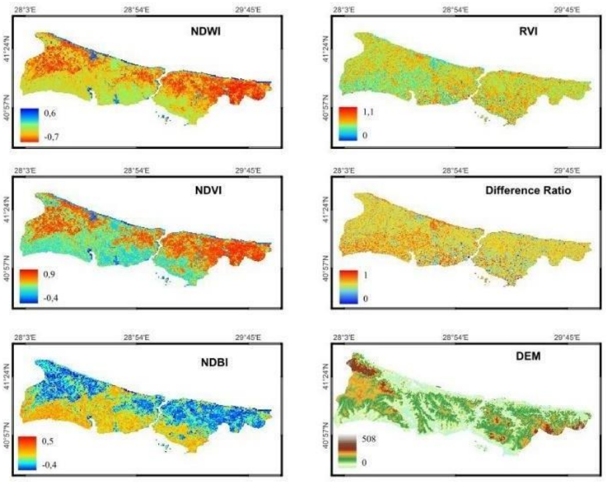

Figure 5. Some of the features derived from Sentinel-1&2.

Figure 6 presents the spatial distribution of the six land-cover classes across Istanbul for 2016. Forest areas are mainly concentrated in the northern parts of the study area and appear as relatively continuous patches, while urban areas are densely distributed around the metropolitan core and coastal zones. Agricultural lands are primarily located in the western and interior regions and often occurring adjacent to forest and urban classes. Bare lands are scattered throughout the region, often located near urban and agricultural areas. Water bodies are clearly delineated along the major reservoirs, whereas roads appear as linear features mostly within urban areas.

The spatial patterns are consistent with the reported accuracy metrics. Producer’s accuracies (PA) were highest for Forest (81%), Urban (79%), and Agriculture (76%), indicating reliable detection of dominant classes. Lower PA values were observed for Bare land (67%), Water (62%), and Roads (62%), suggesting higher omission errors in these categories. User’s accuracies (UA) were highest for Water (84%) and Roads (83%), followed by Forest (72%), Bare land (69%), Urban (67%), and Agriculture (64%). The overall classification accuracy reached 72% (Table 2).

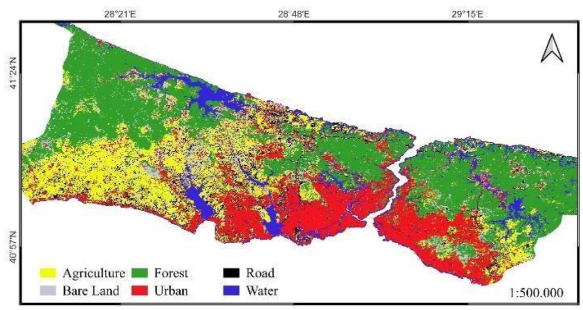

Figure 6. Land-cover classification results of 2016 data.

(%)	*Agriculture*	*Bare Land*	*Forest*	*Urban*	*Road*	*Water*
PA	76	67	81	79	62	62
UA	64	69	72	67	83	84
OA	**72**					

Table 2. Accuracy metrics of 2016 data

Figure 7 presents annual land-cover classification maps from 2017 to 2025, generated using a RF model trained on 2016 data. The maps clearly show the expansion of urban surfaces, particularly along the transition zones between the northern forest corridors and the existing city center. The model successfully detects the conversion of Agriculture and Forest areas into Urban and Bare Land (representing construction sites), maintaining high thematic consistency throughout the ten-year period.

Figure 8 presents the annual area variations (km²) of agriculture - forest, urban - road, water, and bare land classes. The visible decrease in forest and agriculture areas, particularly in the northern regions in the 2024–2025 maps (Figure 7), corresponds to the cumulative forest loss of 379 km² presented in Figure 8. The permanent water bodies in the study area were generally correctly classified (Figure 7). However, the annual area changes observed for this class are mostly the result of misclassifications, caused by sensor and topographical limitations such as shadow effects. Despite these classification errors in the classification results, the overall trend over the 10-years indicates a general decrease in total water areas.

The analysis of the Urban class in Figure 8 provides important insights into urban growth throughout the study period (2016–2025). Corresponding to the decrease in natural areas such as forests, agriculture and water the Urban class shows an increase. As observed in the classification results (Figure 7), urban growth expands from the existing city center to the northern forests and agricultural areas, leading to the gradual loss and change of natural land cover. Additionally, the Bare Land class in Figure 8 shows a continuous trend. The classification results indicate that bare land generally represents a pre-construction stage.

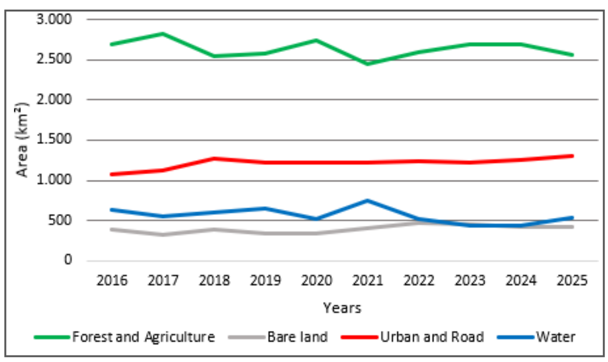

Figure 8. Annual area variations (km²).

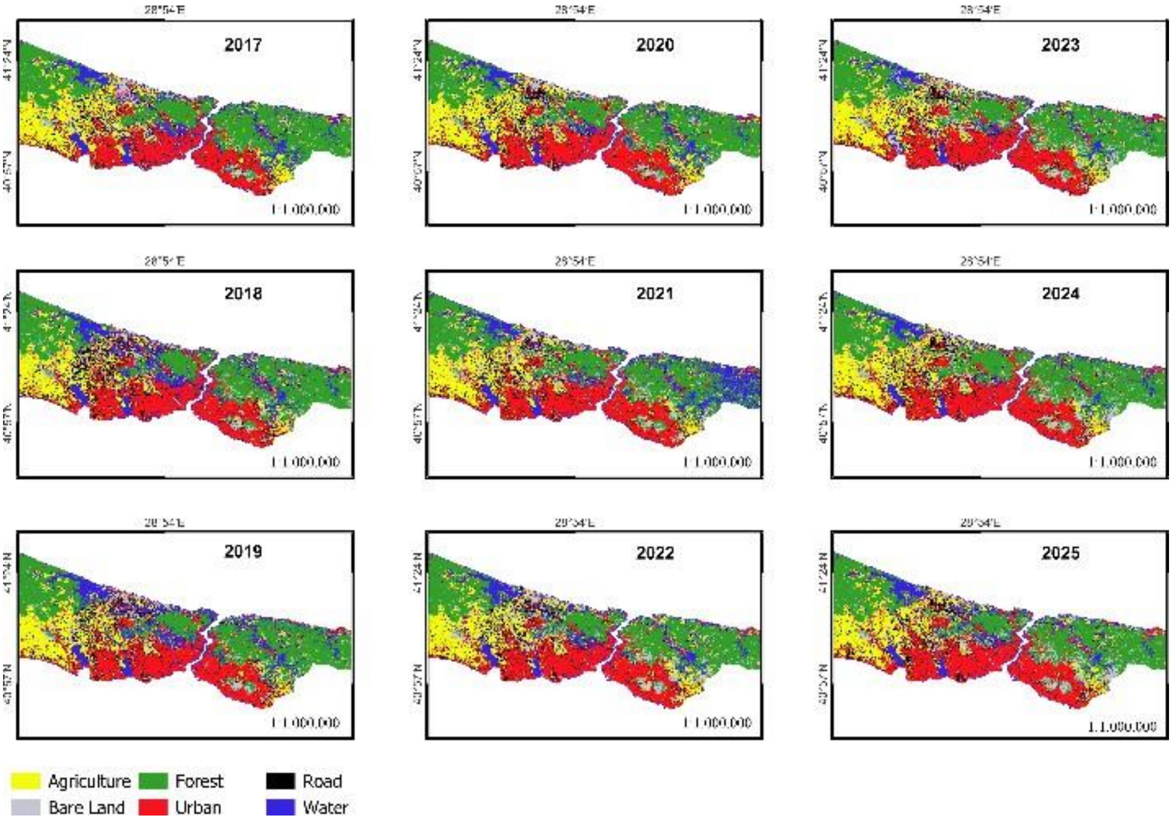

Figure 7. 2017-2025 land-cover classification results using the trained RF model (2016).

4. Conclusion

This study presented a Google Earth Engine-based framework to monitor long-term land-cover changes in the Istanbul metropolitan region from 2016 to 2025. By fusing Sentinel-1, Sentinel-2 and topographic features, the Random Forest model showed significant LULC changes. As a result of the study, the overall classification reached 72% accuracy. Agriculture, Bare Land, and Forest classes were relatively well distinguished, while Road and Water showed more confusion, likely due to their spectral similarities. According to the time-series analysis, the agricultural area declined by 231 km² over 2016–2025, with a comparable reduction of 379 km² observed in the forested area. These findings highlight notable land cover changes within the study area, reflecting both anthropogenic and natural influences on the landscape.

The feature importance analysis indicated that physical and structural variables, particularly DEM and SAR-derived metrics played a major role in the classification process. The contribution of these variables helped the model preserve spatial consistency and detect gradual land-cover changes, such as the changes from vegetation to bare land and to urban surfaces. This structural information also reduced the influence of atmospheric variability affecting optical data.

The lack of annual reference data for continuous model training and validation presents a major limitation in long-term land-cover monitoring. In light of this constraint, a key contribution of this study was analyzing the temporal transferability of a classifier trained on a single baseline year, utilizing LPIS data derived from 2016 high-resolution orthophotos. However, although this approach is practical for monitoring long-term trends, applying a model trained on a single reference year without independent annual validation data may lead to limitations and uncertainties in the classification results.
Future studies should therefore focus on exploring alternative methodological strategies to improve the accuracy and reliability of transferable classification models for long-term LULC monitoring. In addition, integrating longer-wavelength radar datasets, such as L-band (e.g. ALOS PALSAR, NISAR), may further enhance classification performance by enabling deeper canopy penetration and providing improved structural discrimination among complex land-cover types.

ACKNOWLEDGEMENTS

This study was supported by the Scientific and Technological Research Council of Türkiye (TÜBİTAK) under grant number 2224-A.

References

Breiman, L., 2001. Random forests. Machine Learning, 45(1), pp. 5–32. https://doi.org/10.1023/A:1010933404324

Bullock, E.L., Woodcock, C.E., Souza, C., Olofsson, P., 2020. Satellite-based estimates reveal widespread forest degradation in the Amazon. *Global Change Biology*, 26, pp. 2956–2969. https://doi.org/10.1111/gcb.15029

Eisfelder, C., Boemke, B., Gessner, U., Sogno, P., Alemu, G., Hailu, R., Huth, J., 2024. Cropland and crop type classification with Sentinel-1 and Sentinel-2 time series using Google Earth Engine for agricultural monitoring in Ethiopia. *Remote Sensing*, 16(5), 866.

Gorelick, N., Hancher, M., Dixon, M., Ilyushchenko, S., Thau, D., Moore, R., 2017. Google Earth Engine: planetary-scale geospatial analysis for everyone. *Remote Sensing of Environment*, 202, pp. 18–27. https://doi.org/10.1016/j.rse.2017.06.031

Irfan, A., Li, Y., E, X., Sun, G., 2025. Land use and land cover classification with deep learning-based fusion of SAR and optical data. Remote Sensing, 17(7), 1298.

Lehmann, E.A., Caccetta, P., Lowell, K., Mitchell, A., Zhou, Z.S., Held, A., Milne, T., Tapley, I., 2015. SAR and optical remote sensing: assessment of complementarity and interoperability in the context of a large-scale operational forest monitoring system. *Remote Sensing of Environment*, 156, pp. 335–348. https://doi.org/10.1016/j.rse.2014.09.034

Mao, Z., Deng, L., Liu, X., Wang, Y., 2025. A comparative analysis of SAR and optical remote sensing for sparse forest structure parameters: a simulation study. Forests, 16(8), 1244. https://doi.org/10.3390/f16081244

Menze, B.H., Kelm, B.M., Masuch, R., Himmelreich, U., Bachert, P., Petrich, W., 2009. A comparison of random forest and its Gini importance with standard chemometric methods for the feature selection and classification of spectral data. BMC Bioinformatics, 10, 213. https://doi.org/10.1186/1471-2105-10-213

Ozdemir, E.G., Abdikan, S., 2024. Estimating forest above-ground biomass using Sentinel-2 and SDGSAT-1 with predictive regression models. International Workshop on Metrology for Agriculture and Forestry (MetroAgriFor), pp. 660–665.

Purnam, K.K., Prasad, A.D., Ganasala, P., 2024. Water indices for surface water extraction using geospatial techniques: a brief review. Sustainable Water Resources Management, 10(2), 70.

Reiche, J., Hamunyela, E., Verbesselt, J., Hoekman, D., Herold, M., 2018. Improving near-real time deforestation monitoring in tropical dry forests by combining dense Sentinel-1 time series with Landsat and ALOS-2 PALSAR-2. Remote Sensing of Environment, 204, pp. 147–161. https://doi.org/10.1016/j.rse.2017.10.034

Simsek, F.F., Durduran, S.S., 2023. Land cover classification using Land Parcel Identification System (LPIS) data and open source EO-Learn library. Geocarto International, 38(1), 2146760. https://doi.org/10.1080/10106049.2022.2146760

Van Tricht, K., Gobin, A., Gilliams, S., Piccard, I., 2018. Synergistic use of radar Sentinel-1 and optical Sentinel-2 imagery for crop mapping: a case study for Belgium. Remote Sensing, 10(10), 1642. https://doi.org/10.3390/rs10101642

Watanabe, M., Koyama, C.N., Hayashi, M., Nagatani, I., Tadono, T., Shimada, M., 2021. Refined algorithm for forest early warning system with ALOS-2/PALSAR-2 ScanSAR data in tropical forest regions. Remote Sensing of Environment, 265, 112643. https://doi.org/10.1016/j.rse.2021.112643

Yan, K., Gao, S., Yan, G., Ma, X., Chen, X., Zhu, P., Wang, Q., 2025. A global systematic review of the remote sensing vegetation indices. International Journal of Applied Earth Observation and Geoinformation, 139, 104560.
Ye, S., Rogan, J., Zhu, Z., Eastman, J.R., 2021. A near-real-time approach for monitoring forest disturbance using Landsat time series: stochastic continuous change detection. Remote Sensing of Environment, 252, 112167. https://doi.org/10.1016/j.rse.2020.112167

Zhang, R., Qiu, J.S., Yang, Z., Li, T., Yang, X., 2022. Near-real-time monitoring of land disturbance with harmonized Landsats 7–8 and Sentinel-2 data. *Remote Sensing of Environment*, 278, 113073. https://doi.org/10.1016/j.rse.2022.113073

Zhu, Z., Zhang, J., Yang, Z., Aljaddani, A.H., Cohen, W.B., Qiu, S., Zhou, C., 2020. Continuous monitoring of land disturbance based on Landsat time series. Remote Sensing of Environment, 238, 111xxx. https://doi.org/10.1016/j.rse.2019.03.009